RSC Advances

This article can be cited before page numbers have been issued, to do this please use: N. Riaz, C. F. Kait, Z. Man, R. Sarwar, U. Farooq, A. Khan and M. S. Khan, *RSC Adv.*, 2016, DOI: 10.1039/C6RA10371E.

ROYAL SOCIETY OF CHEMISTRY

www.rsc.org/advances

View Article Online
DOI: 10.1039/C6RA10371E

Journal Name

ARTICLE

Preparation, characterization and application of Cu-Ni/TiO_2 in Orange II photodegradation under visible light: Effect of different reaction parameters and optimization

Received 00th January 20xx,
Accepted 00th January 20xx

DOI: 10.1039/x0xx00000x

www.rsc.org/

Nadia Riaz,[a,†] F. K. Chong,[b,†] Z. B. Man,[c] R. Sarwar,[d] U. Farooq,[d] A. Khan[d] and M. S. Khan[a]

BimetallicCu-Ni/TiO_2photocatalysts were prepared using wet impregnation method. The physicochemical and morphological properties of the photocatalsyts were studied using different characterization techniques. FTIR analysis showed the nitrate peaks are still present but did not showed effect on the catalytic performance of the photocatalysts. Photocatalysts were nanosize and morphologies are spherical and slightly agglomerated. From DRUV-Visible analysis, it was proved that incorporation of Cu and Ni onto TiO_2 has successfully shifted the optical absorption to the visible region with reduced bandgap energies. Furthermore, increasing the calcination temperature bandgap energy was reduced. The lowest band gap energy (2.74 eV) was reported for 9Cu:1Ni-300. Photocatalytic degradation Orange II was studied under visible light. The photocatalyst performance of bimetallic Cu-Ni/TiO_2 for Orange II decoloration and mineralization is promising compared to bare TiO_2 and the monometallic photocatalysts. Compared to other Cu:Ni mass compositions, results for photodegradation studies showed that 9Cu:1Ni mass composition was observed with 100 % Orange II decoloration and 89.8% and 100% TOC removal in 1h and 1.5 of irradiation duration, respectively. The optimum pH value was 6.8. The main identified intermediates and by products of Orange II photodegradation under visible light irradiation during reaction as a function of time were oxalic acid, formic acid, formaldehyde, benzyl alcohol and benzaldehyde as measured by HPLC analysis.

Introduction

The textile industry is the major contributor responsible for the aquatic ecosystems pollution due to the generated wastewaters. Such industrial effluents are highly colored and their release in the ecosystem is a dramatic source of aesthetic pollution and perturbation in the aquatic life. For this reason, the international environmental standards become more and more stringent[1-3]. Azo dyes are the largest group of dyes, constituting 60–70% of all dyestuffs produced and used in textile industry[4, 5].Orange II was used as model azo dye, an anionic monoazo textile dye of the acid class. The high stability of Orange II is useful in textile manufacturing due to its resistant to light degradation, action of O_2 and common acids or bases but problem arises later due to difficulty in managing its removal from the wastewaters. Treatment of residual dyes has been an important issue of research. Although textile dyes can be disposed via some physical and chemical processes, these methods are usually incomplete and ineffective. Orange II does not undergo biological degradation[6]. Additionally, biological processes exhibited limited efficiency due to xenobiotic and non-biodegradable characteristics of textile dyes. Furthermore, some physical and chemical treatments can generate secondary pollution resulting from toxic products[7].

Semiconductor photocatalysis has been investigated extensively for light-stimulated degradation of pollutants[8-14]. Several semiconductors exhibit band-gap energies suitable for photocatalytic degradation of contaminants. Among the photocatalysts applied, titanium dioxide (TiO_2) is one of the most widely employed photocatalytic semiconducting materials because of the peculiarities of chemical inertness, non-photocorrosion, low cost and non-toxicity. Carp et al.,[9] pointed out that doping semiconductors with various metal ions, composite semiconductors, deposition of group VIII metals, and oxygen reduction catalysts can be employed to enhance photocatalytic efficiency.

The use of Cu and Ni as bimetallic catalyst supported on different semiconductor materials has been reported as the effective method to improve the efficiency of various reactions like carbondioxide hydrogenation[15], steam reforming of methane[16], Liquid-phase

[a] Department of Environmental Sciences, COMSATS Institute of Information Technology, Abbottabad, Pakistan.
[b] Fundamental&Applied Sciences Department, Universiti Teknologi PETRONAS, Tronoh, Malaysia
[c] Chemical Engineering Department, Universiti Teknologi PETRONAS, 31750 Tronoh, Malaysia
[d] Department of Chemistry, COMSATS Institute of Information Technology, Abbottabad, Pakistan

†Correspondence: nadiariazz@gmail.com; chongfaikait@petronas.com.my

glycerol hydrogenolysis by formic acid over Ni–Cu/Al_2O_3 catalysts[17], decomposition of methane over Ni-SiO_2 and Ni-Cu-SiO_2 catalysts[18] and for photocatalytic reduction of nitrate[19]. Only few studies have been reported using Cu, Ni or Cu-Ni photocatalysts for azo dye degradation like Cu-Zn/TiO_2[20], Ni/TiO_2[21] and Cu-Fe/TiO_2[22] for methyl orange degradation and Cu/TiO_2 for Orange II degradation with 90% color removal in the presence of UVC light and O_2 after 150 min reaction[23].

In our previous studies Cu-Ni/TiO_2 photocatalysts were prepared employing deposition-precipitation (DP) method[24] and modified co–precipitation method (CP)[25]. Depending on the method of preparation and calcination temperatures have prominent influence on the activity of the prepared photocatalysts. In comparison to our previously reported methods, WI photocatalysts displayed the best performance for Orange II decoloration among DP and CP photocatalysts. Higher calcination temperature (300ºC) resulted TiO_2 photocatalysts with lower bandgap energy 2.74 eV for WI-9Cu;1Ni-300 and high crystallinity. The addition of metals onto the surface of TiO_2 has effectively led to the better photocatalytic performance for Orange II photodegradation under visible light irradiation effectively as compared to the blank experiment without adding any photocatalyst indicating the merely photolysis.

The present work deals with the bimetallic TiO_2 photocatalyst preparation via wet impregnation method (WI). The introduction of Cu and Ni was with the intention to reduce the band gap of the photocatalyst for enhanced visible light absorption. The objective of present study was to determine the photocatalytic activity of bimetallic Cu-Ni/TiO_2 for Orange II photodegradation under visible light source, using Orange II as a model azo dye. Different parameters studied were; different Cu:Ni mass composition, metal loading and the effect of calcination temperatures on the photocatalyst performance. The photocatalysts were further characterized using different characterization techniques to understand the chemical and physical properties and then to relate these properties to their photocatalytic performance.

Experimental

Materials

Copper nitrate trihydrate, $Cu(NO_3)_2.3H_2O$ and nickel nitrate hexahydrate, $Ni(NO_3)_2.6H_2O$ (Acros brand >98% purity) were used as dopant metal salts. Titanium dioxide, TiO_2 (Degussa P25 80% anatase, 20% rutile) was used as the support which also acts as the semiconductor in photocatalysis. Orange II (Acros, pure) was used as the model azo dye for photocatalytic degradation study. The chemical structure and specifications of Orange II are shown in S1.(see supplementary materials). All chemicals were used as received.

Photocatalyst preparation

A series of bimetallic Cu-Ni/TiO_2 photocatalysts with different total metal loading (5, 10 and 15 wt%) and different mass composition of copper to nickel (10:0, 9:1, 7:3, 5:5, 3:7, 1:9 and 0:10) were prepared using wet impregnation (WI) method with TiO_2 as support. To prepare photocatalysts using WI method, support was added into the metal salt solution. The suspension was stirred for 1 hour before the solvent was evaporated in a water bath at 80ºC until a thick paste was obtained. This paste was then dried in an oven at 120ºC for 18 hours. The dried photocatalyst was ground with a mortar and pestle, kept in air-tight glass bottle as raw photocatalyst and stored in a desiccator at room temperature prior to calcination.

Photocatalyst Characterization

It is important to characterize the calcined photocatalysts in order to determine mainly their chemical and physical properties and then to relate these properties to their photocatalytic performance. The thermal stability of the raw photocatalysts was determined by thermal gravimetric analysis (Perkin Elmer, Pyris 1TGA) instrument. The dried photocatalyst was loaded in a sample cup and weighed using a built-in microbalance attached to the instrument which automatically provides the weight of the sample (in the range of 5-10 mg). The sample was heated in flowing N_2 as background atmosphere from 30°C to 800°C at a ramp rate of 20°C/min. Fourier Transform Infrared spectroscopy (FTIR, Shimadzu FTIR-8400S) analyses was carried out to identify species present in the photocatalysts. A small amount of photocatalyst was grained together with 50 mg of IR-grade KBr and pressed into pellet using a hydraulic hand press. Later the pellet was placed in the sample holder and scanned at 4000 cm^{-1} to 400 cm^{-1}. KBr was used as the background file. Point of zero charge (PZC) was determined by mass titration method [26]. Photocatalysts were weighted and mixed with distilled water to give concentration of 0.1, 0.5, 1, 2, 5 and 10 % (w/v). The suspensions were agitated for 24 h to equilibrate the adsorption-desorption processes, after which pH of the suspensions were determined using pH meter. PZC was estimated by measuring the pH at which further addition of solid catalyst did not change the pH of the suspension. The crystal phases present in the prepared photocatalysts were investigated using X-ray diffractometer (XRD, Bruker D8 Advance Diffractometer), with CuKα radiation (40 kV, 40 mA) at 2θ angles from 10° to 80°, with a scan speed of 4°min^{-1}. The morphology of the photocatalysts such as crystallite particle shape and size distribution wereanalyzed using FESEM (Supra55VP) and HRTEM (Zeiss Libra 200). The Brunauer-Emmett-Teller (BET) analysis was conducted to determine surface area and pore size distribution of the photocatalyst by adsorption of nitrogen at 130 °C, by using a Micromeritics ASAP 2000 instrument. Reflectance spectrums were recorded at 190–800 nm wavelength using DR-UV-Vis. Spectrophotometer (Shimadzu Lambda 900). The band gap energies of the photocatalysts were determined from the reflectance using Kubelka-Munk function, F(R), and the extrapolation of Tauc plot, which is a plot of $(F(R).h\nu)^{1/2}$ against hν. F(R) is Kubelka-Munk function which derived from reflectance spectra following $F(R) = (1-R)^2/2R$ equation, and hv is the photon energy. Barium sulphate (Ba_2SO_4) powder was used as a standard, an internal reference. The temperature programmed reduction (TPR) analyses were conducted in order to determine reducibility of the photocatalysts and metal dispersion in photocatalysts using ThermoFinnigan

View Article Online DOI: 10.1039/C6RA07715

equipment (TPDRO 1100). Prior to reduction, the sample was pretreated under nitrogen at 110 ºC with a flow rate of 20 mLmin^{-1} and ramp rate of 10 ºC min^{-1}, and finally holding at 110 ºC for 30 minutes to eliminate moisture before cooling to room temperature. TPR analysis was carried out in 5% H_2 in N_2 with a flow rate of 20 mL min^{-1}. Sample were heated with a ramp rate of 20 ºC min^{-1} from 40 ºC-500 ºC and holding at 500 ºC for 10 minutes. The reduction profile was showed in a plot of hydrogen consumption as a function of linearity temperature.

Measurements of photocatalytic activities

Photocatalytic activity of the prepared photocatalysts was evaluated by monitoring the photocatalytic degradation of Orange II in aqueous solution under visible light irradiation. For a typical experiment, photocatalysts were weighed and mixed with distilled water and then ultrasonicated for 10 min using an ultrasonicator. Afterwards, Orange II solution was added with a final concentration of 50ppm with photocatalyst loading 1 g·L^{-1} and total volume of 30 ml. The suspension was stirred using a magnetic stirrer for in the dark (2 h) and later this suspension was illuminated for 1 h using the 500 W halogen lamp as the visible light source at a distance of 25 cm (46.1615 W·m^{-2}). Reaction study was carried out at atmospheric pressure and room temperature (at 25±2^{o}C) that was controlled by continuous cooling air. Prior to absorbance measurement (at wavelength of 485 nm, corresponding to maximum absorption wavelength of Orange II), the reaction samples were immediately centrifuged twice at 3500 rpm for 10 min to remove suspended solid photocatalyst and monitored for the remaining Orange II concentration and further analysis. Orange II specifications, the model azo dye, and the experimental setup used for photodegradation are shown in S1 and S2, respectively (see supplementary materials).

The degradation of a dye can be characterized in two ways: percent decoloration and percent mineralization. Decoloration refers to the reduction in concentration of the parent dye molecule under consideration at its characteristic wavelength, but does not refer to the complete removal of the organic carbon content. This is due to the formation of colored dye intermediates, which absorb at different wavelengths. Hence, complete degradation or mineralization occurs when all the organic carbon is converted to CO_2. Therefore, analyzing the mineralization of the dyes in terms of the total organic carbon (TOC) content assumes importance. TOC is the amount of carbon bound in an organic compound and is often used as a non-specific indicator of water quality or cleanliness of pharmaceutical manufacturing equipment. A typical analysis for TOC measures both the total carbon present as well as the so called "inorganic carbon" (IC), the latter representing the content of dissolved carbon dioxide and carbonic acid salts. Subtracting the inorganic carbon from the total carbon (TC - IC) yields TOC. A total organic carbon analyzer (V_{CSH} Shimadzu Co.) was used to measure the TOC concentration (ppm) for the reaction samples.

In order to determine the decoloration efficiency of photocatalyst, Orange II decoloration (%) was calculated as follows:

$$Orange\ II\ decoloration\ (\%) = \left(\frac{C_o - C_t}{C_o}\right) \times 100 \qquad (1)$$

where: C_o = initial concentration of dye in ppm and C_t is the concentration of dye at different time intervals during reaction in ppm. At the end of a particular reaction, centrifuged samples were further analysed for the total organic carbon (TOC). The TOC removal (%) was calculated as follows:

$$\text{TOC removal}(\%) = \left(\frac{TOC_o - TOC_f}{TOC_o}\right) \times 100 \qquad (2)$$

where: TOC_o = initial TOC in ppm and TOC_f = final TOC in ppm.

High Performance Liquid Chromatography Analysis (HPLC)

Orange II photodegradation products were analyzed using high performance liquid chromatography (HPLC Agilent 1100 series) equipped with auto sampler. The analysis was carried out using a Zorbex SB- C18 5um, 150 mm x 10 mm column with a Mobile phase 70:30 aqueous solution of ammonium acetate (20 mM) and acetonitrile at a flow rate: 1 mL.min^{-1}, while retention time was 20 min at ambient temperature. The injection volume was 5 µL, room temperature 22.2°C, column temperature 26.6°C and 117 bar pump pressure. Detector was operated at three different wavelengths 485nm, 254nm and 215nm (DAD-UV Lamp). Standard solutions were prepared in the eluent with different known concentrations. Some intermediates[27, 28] products[29, 30] of Orange II photodegradation were used as standards for analysis and the results were used to determine their compositions during reaction. The standards are benzyldehyde (99.5%, Fluka), benzyl alcohol (Fluka), formaldehyde (Assay ≥ 36.5 %) and formic acid (≥ 98%), oxalic acid (≥ 99.0%, Fluka), propionic acid (≥ 99.8%), sulfanilic acid (≥ 99.0%, Fluka), 2-naphthol (99 %, Aldrich). Calibration curves were obtained for all the standards with known concentrations.

Results and Discussions

Resultsfrom TGA were reported as thermograms which are plots of the relative weight of the photocatalyst versus temperature. The calcined photocatalysts were given denotation: xCu–yNi–T (the dash is from insert symbol) where 'x' and 'y' represent the mass composition of Cu and Ni, respectively, with 'x'+'y'=10; while 'T' represents calcination temperature in °C.

Photocatalyst characterization

Thermal analysis. Prior to calcination, pre-treatment of the raw photocatalysts was carried out to estimate the suitable calcination temperatures to activate the raw photocatalysts material. This step was conducted to monitor the decomposition temperature of the photocatalysts at which the raw photocatalyst began to decompose and the temperature range at which the photocatalyst has achieved thermal stability. The thermogram of the raw photocatalyst (10 wt%-9Cu:1Ni) is shown in Figure 1. The TG curves showed two decomposition steps: the first weight loss step (30 to 150^{o}C) depicts the evaporation of physically adsorbed water [31-33] while thesecond abrupt step from 150 to 400^{o}C and onwards represents the decomposition of the $Cu(NO_3)_2$ and $Ni(NO_3)_2$, to form copper oxide, CuO[31] and NiO, respectively. Total weight loss was

26.45% (S3). Proposed decomposition steps for the raw WI photocatalyst are shown in Equations 3 and 4.

$$Cu(NO_3)_2 \rightarrow CuO_{(s)} + 2NO_{2\,(g)} + O_{2\,(g)} \quad (3)$$

$$Ni(NO_3)_2 \rightarrow NiO_{(s)} + 2NO_{2\,(g)} + O_{2\,(g)} \quad (4)$$

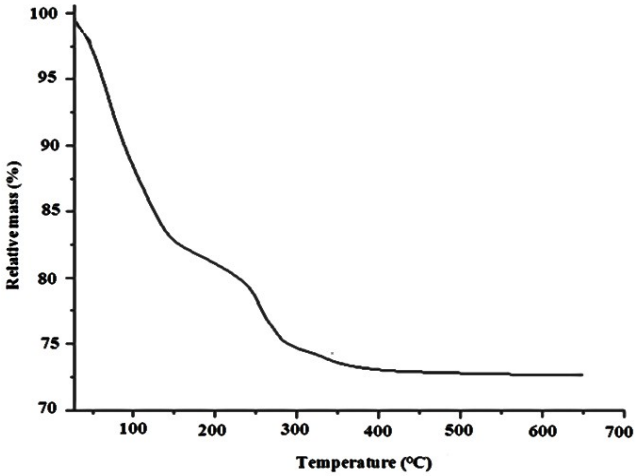

Fig.1 The thermogram of the raw photocatalyst (10 wt%-9Cu:1Ni)

From 400°C onwards there was a straight horizontal line, indicating no further decomposition and the photocatalyst was thermally stable.

Fourier Transform Infrared Spectroscopy (FTIR). FTIR spectra of 10wt% 9Cu:1Ni-200 photocatalysts is shown in S4. Bare TiO_2, raw and calcined photocatalysts (at 180°C, 200°C and 300°C) were compared. Several absorption peaks were observed. The broad band around 3400 cm^{-1} was attributed to O–H stretching, and the peak near 1600 cm^{-1} to H–O–H bending and related to physically absorbed moisture [31, 34]. The IR band observed from 400–900 cm^{-1}corresponds to the Ti-O stretching vibrations[35-37]. Similar results were displayed by the photocatalysts calcined at 180°C and 300°C. The intense peak at 1384 cm^{-1} was ascribed to nitrate (NO_3^-) group which is present in all the spectra. The presence of nitrate band was also observed by Mohan [38], Li and Inui [39]. They mentioned that the nitrate will always be present when nitrate salts are used as precursors. Since the color of the calcined photocatalysts was different compared to the raw photocatalysts but not the same as the color of the oxides, it can be deduced that the calcination conditions were not enough to remove completely the nitrates. However, in the present study, the presence of nitrate anions in photocatalysts did not affect the catalytic activity of the photocatalysts. Possible assignment of the peaks observed in FTIR spectra of bare TiO_2 and Cu:Ni/TiO_2 photocatalysts is shown in S5.

Point of Zero Charge determination. PZC is defined as the pH at which the net charge is zero, at which coverage of the H^+ equals the coverage of OH^-. In the present study, PZC was determined by mass titration method. Plots of pH versus mass percentage WI-9Cu:1Ni-200 and bare TiO_2 are shown in Figure 2. Surface change of the oxide is a result of the acid-base equilibrium. It is a function of pH and ionic strength of the solution. It is necessary to determine the property of the photocatalyst-solution interface as the research on the photocatalyst is intended for the degradation of dyes in aqueous solution. For the photocatalyst samples containing Cu and Ni, the PZC shifts to more basic values. The PZC value of the Cu-Ni/TiO_2 photocatalysts in the present study is towards alkaline (7.7). The loading of metal oxides onto the surface of TiO_2 can remarkably change the PZC values. PZC for TiO_2 was about 3.8 comparable to those reported in the literature for TiO_2 at 3.5- 6.5[40].

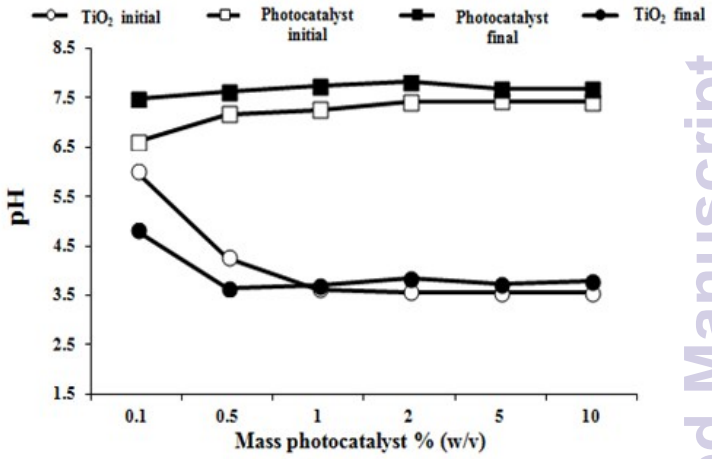

Fig.2 Plot of pH versus the photocatalyst/water mass percentage for TiO_2 and WI-9Cu:1Ni/TiO_2 photocatalyst

If the pH of the suspension is lower than PZC, the surface charge is positive. On the other hand if pH is higher than PZC, the surface charge is negative [26].These results are in agreement with Di Paola et al. [26, 41], who reported that for samples containing Co, Cu and Fe, the PZC moves to more basic values compared to that of the support (PZC 7.1). Di Paola et al.[26, 42], suggested the PZC value of 7.1 for TiO_2. This could be due to the difference in the synthesis procedure as PZC value can be affected by heat treatment on TiO_2.

X- Ray Powder Diffraction (XRD). The XRD patterns of the bare TiO_2 and Cu-Ni/TiO_2photocatalysts calcined at different calcination temperature are shown in Figure 3. Two main phases were observed: anatase and rutile. The peaks at 2θ = 25.34° and 2θ = 27.46° appeared for bare TiO_2 as well as Cu-Ni doped photocatalysts, corresponding to the main peak of anatase and rutile, respectively [31, 43-45]. However, no diffraction lines of Cu or Ni containing phases were observed indicating that the dopants were well dispersed onto TiO_2. Zhu et al. [46], reported that TiO_2 with metal dopant concentration above 5wt% could display small peaks attributable to a separate oxide phase in addition to the peaks for anatase TiO_2. The metal dispersion is confirmed by the results displayed from FESEM-EDX images.

A major variable in photocatalyst preparation is the calcination temperature or subsequent thermal treatment because it affects the resulting TiO_2 crystalline phase, its porosity and surface area [47]. In the calcined samples, no phase transition from anatase to rutile was observed. This might be due to the low calcination temperature as the transition of anatase to the rutile phase normally occurs at

temperature above 600°C. Lopez et al. [48], indicated that the phase transition temperature from anatase to rutile started at calcination temperature about 550°C and complete conversion to the rutile phase was realized at 900°C. However in the current work the highest calcination temperature was 300°C and no phase transformation was observed.

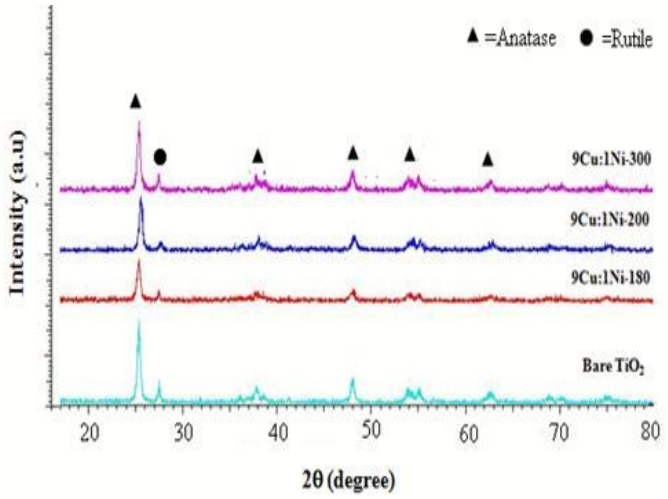

Fig.3 XRD patterns of bare TiO_2 and 9Cu-1Ni/TiO_2 calcined at different temperatures (180, 200 and 300°C)

Field Emission Scanning Electron Microscopy (FE-SEM) and High Resolution Transmission Electron Microscopy (HRTEM). Field Emission Scanning Electron Microscopy (FESEM) was used to evaluate the surface morphologies of photocatalyst such as crystallite shape, size, and metal dispersion. Energy Dispersive X-Ray Spectroscopy (EDX) is used to qualitatively and quantitatively analyze the elements present in a selected area of the FESEM image. The morphology of Cu-Ni/TiO_2 photocatalysts as analyzed by HRTEM and FESEM microscopy, was observed with typically spherical particles of nanometer size and the photocatalysts samples is partly composed of clusters containing composite nanoparticles adhering to each other, slightly agglomerated ranging from 10- 40 nm. The agglomeration may be due to sintering during calcination process. FESEM micrographs of WI-Cu-Ni/TiO_2 photocatalysts (100nm, at magnification 150KX) are shown in Figure 4.

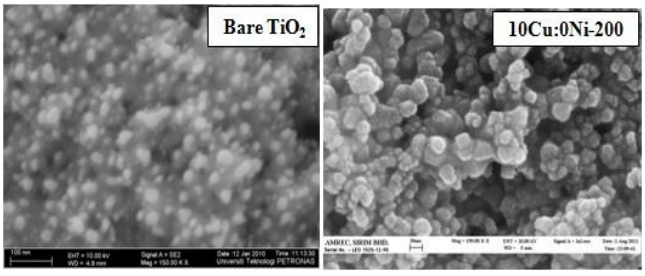

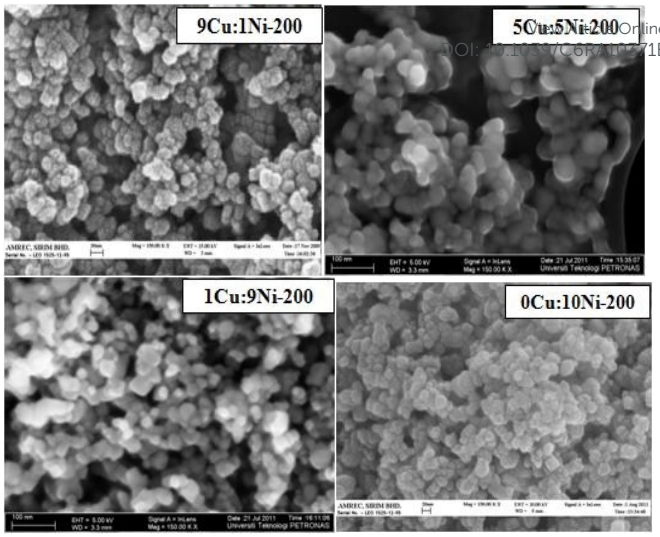

Fig.4 FESEM micrographs of Cu-Ni/TiO_2 photocatalysts (100 nm, at magnification 150KX)

Elemental mapping of the 10wt%-WI-9Cu:1Ni-200 photocatalyst is shown in Figure 5. The respective elements detected in EDX were shown as colored spots in the mapping images. Although the presence of copper, nickel, or both copper and nickel alloy were not detected by XRD, but from the results it is very clear that the small clusters of doped metal (copper and nickel) were highly dispersed and incorporated onto TiO_2 surface. Similar morphology with spherical shape and agglomeration of metal particle was also observed by Riaz et al.[24,25, 49] and Nurlaela et al. [50] for Cu-Ni/TiO_2 while Yoong et al.[31] for Cu/TiO_2 photocatalyst. The highly dispersed metal particle on TiO_2 led to better activity thus further enhances the photocatalytic activity[51].

View Article Online
DOI: 10.1039/C6RA10371E

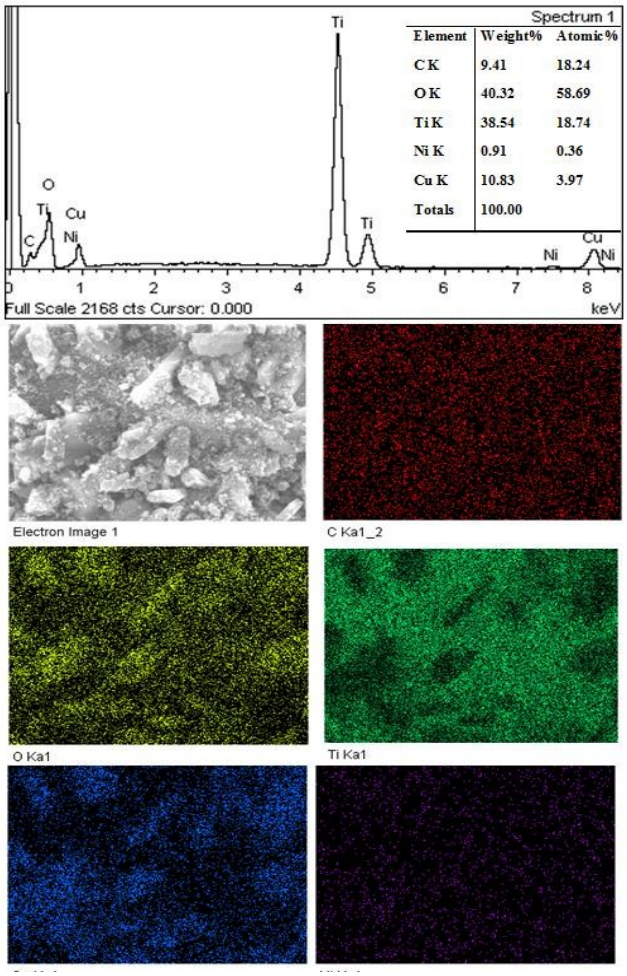

Fig.5 EDX and Mapping image of 10wt% -WI-9Cu:1Ni-200

HRTEM micrographs of the Cu-Ni/TiO_2 photocatalysts (Figure 6) showed a very good crystalline morphology of the particles with different crystallite shapes. The particle size was from 11–35 nm for Cu-Ni/TiO_2 photocatalyst while 11nm–35 nm for bare TiO_2.

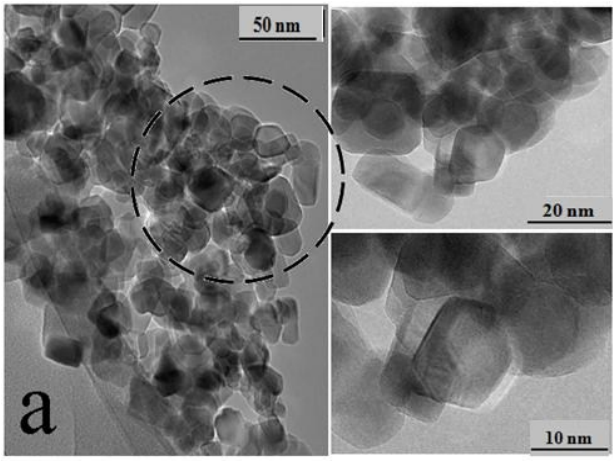

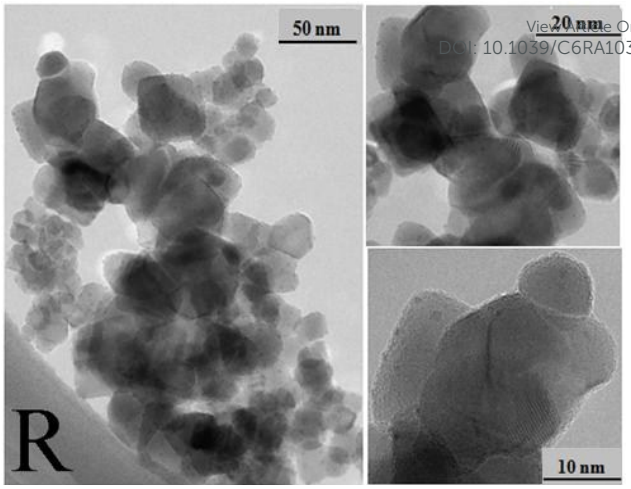

Fig.6 HRTEM micrographs of (a) fresh 9Cu:1Ni-200 and (R) recycled 9Cu:1Ni-200 photocatalysts

Surface Area and Porosity Analysis. The BET surface area, pore volume, and pore diameter of bare TiO_2 and 10wt% photocatalysts with different Cu:Ni mass composition are shown in the Table 1 while the isotherm plots are shown in Figure 7. The N_2 adsorption-desorption isotherm for all the Cu-Ni/TiO_2 photocatalysts showed IUPAC of type IV pattern with H1 hysterisis loop indicating capillary condensation in mesoporous adsorbate[52, 53]. TiO_2 however, displayed type III pattern, which is typically ascribed to non-porous products with weak interactions between the adsorbent and the adsorbate. The surface area of the photocatalysts was found to decrease slightly due to the increase in calcination temperature. Figure 8 shows the pore size distribution of 10wt%-9Cu:1Ni-200, the sharp decline in desorption curve may be a good indicator of the non-uniform pore size of this specimen[54]. The values for BET surface area, pore volume, and pore diameter of Cu-Ni/TiO_2 photocatalysts is shown in Table 2.

In terms of calcination temperature, the surface area and pore volume decreases with increasing temperature while average pore diameter of photocatalyst increase as the temperature increases. However, the high metal dispersion on the TiO_2 surface was reported when the total surface area of photocatalysts was increased [55].

Table 1 BET surface area, pore volume, and pore diameter of Cu-Ni/TiO_2 photocatalysts

Photocatalyst	Surface area ($m^2 \cdot g^{-1}$)	Total pore volume ($cm^3 \cdot g^{-1}$)	Average pore diameter (nm)
Bare TiO_2	43.1	0.20	18.5
WI-9Cu:1Ni-180	72.2	0.43	23.9
WI-9Cu:1Ni-200	35.7	0.24	26.4
WI-9Cu:1Ni-300	46.3	0.32	27.4

Different Cu:Ni calcination temperatures

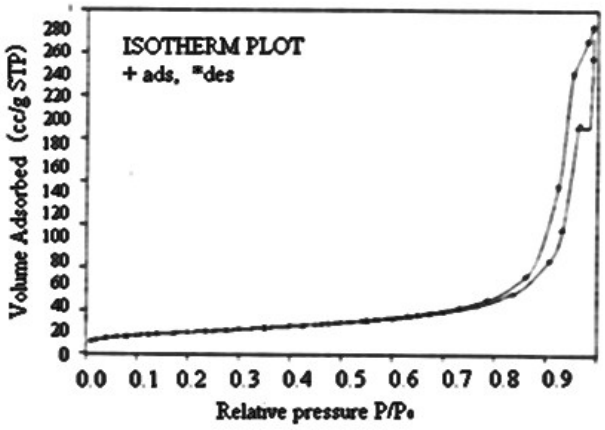

Fig.7 Isotherm plot for 10wt%-WI-9Cu:1Ni-200

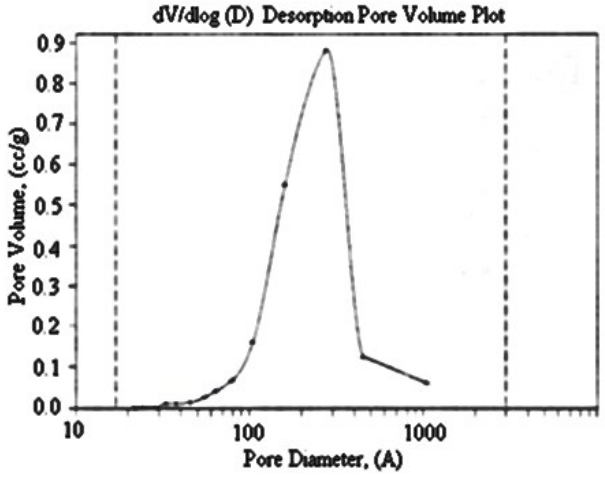

Fig.8 Pore size distribution of 10wt%-WI-9Cu:1Ni-200

Diffuse Reflectance UV-Visible Spectroscopy (DR-UV-Vis). The DR-UV-Vis absorption spectrum of bare TiO_2 and photocatalysts with different calcination temperature are presented in (S6-a). Modification with metal can shift the absorption spectrum of TiO_2into visible region. The shift in the absorption spectrum has been observed for the synthesized photocatalysts. Impregnation method has also been reported previously that this method can also shift the absorption spectrum of TiO_2 [42]. The shift is not possibly caused by the change in the bandgap, but rather by the impurity of energy level as the metal is spread on the surface of TiO_2 and not incorporated into TiO_2 framework. Nevertheless, bulk properties of TiO_2 are as important as surface properties of TiO_2 [56]. The DR-UV-Vis spectra of bare TiO_2 showed absorption peaks ranging from 190 nm and 400 nm, similar to that observed in our previous studies [24, 31, 50]. The absorption at 323 nm is generally related to the electronic excitation from the valence band O 2p electron to conduction band Ti 3d orbital indicating the Ti is in the form of tetrahedral Ti^{4+} species [57]. Better activity of the photocatalysts was reported which clearly shows that the surface modification of TiO_2 Cu-Ni, has significantly enhanced the absorption properties of photocatalyst. Calcination temperature and duration play important role in shaping the characteristics and activities of the photocatalysts. In terms of calcination temperature it was found that with an increase in the calcination temperature there was a decrease in the bandgap energy of the photocatalyst was observed (S6-b). The calculated bandgap energies for bare $TiO_2$was 3.16eV while 2.96, 2.95 and 2.74eV for photocatalysts calcined at different temperature 180, 200 and 300°C, respectively. This statement suggested that different calcination temperature affected the bandgap energy as proposed by Sakhtivel et al. [58].

Temperature Programmed Reduction (TPR). Temperature Programmed Reduction (TPR) was used in order to characterize the Cu-Ni/TiO_2 photocatalyst with respect to the type of metal oxide species present, either copper oxide, nickel oxide, or copper-nickel mixed oxide, and the degree of interaction of the oxides with TiO_2 support [31]. The summary of the amount of hydrogen consumed and reduction temperature of different photocatalysts is shown in Table 2. The TPR profiles of the bimetallic 9Cu:1Ni/TiO_2 photocatalysts with different calcination temperature are presented in S7. The higher reduction peaks at 295°C was ascribed to bulk CuO phases that include large clusters and bulk CuO. The reduction profile of bimetallic 9Cu:1Ni-200 showed a shoulder around 220–240°C and one main reduction peaks, 289°C, that might be attributed to the reduction of Cu–Ni mixed oxide instead of individual oxide. Higher reduction temperatures are attributed to the reduction of NiO with strong interaction with TiO_2[59]. The distinct peak observed at 289°C for 9Cu:1Ni-180 might be attributed to the reduction of Cu-Ni mixed oxide instead of individual oxide [55]. It was also found that the presence of Cu lowered the reduction temperature of Ni. Li et al. [60], observed the same behavior as the bimetallic Cu-Ni/TiO_2. The addition of Cu enhanced the reduction of Ni, thereby it can be concluded that the reducibility of bimetallic Cu–Ni is controlled by the amount of Cu. However, the presence of Cu–, Ni–, as well as mixed Cu–Ni species were not detected by XRD analysis due to high dispersion of the metal particle on TiO_2. The TPR profile of monometallic Cu/TiO_2 was in good agreement with the results showed by the XRD and FESEM, that the Cu- species was highly dispersed on TiO_2 photocatalyst.

Table 2 Summary of the hydrogen consumption and the reduction temperature of the photocatalysts

Photocatalyst	Reduction peak (°C)	Amount of hydrogen consumed (μmol·g^{-1})
WI-9Cu:1Ni-200	289	1879.3
	357	1938.2
WI-9Cu:1Ni-180	295	1877.0
	361	1939.9
WI-9Cu:1Ni-300	216	345.79
	276	1436.2
	355	158.98

Photocatalytic activity of Cu-Ni/TiO_2 photocatalysts

Cu:Ni mass compositions. By fixing the total metal loading, 10 wt% Cu-Ni/TiO_2 photocatalysts prepared with different Cu-Ni mass compositions calcined at 200°C were studied for Orange II decoloration at pH 6.8. Bimetallic photocatalysts with 9:1, 5:5 and 1:9 Cu:Ni mass compositions were observed with highest percentage of Orange II decoloration compared to mono metallic and bare TiO_2. In case of different Cu:Ni mass compositions 9Cu:1Ni-200 photocatalysts showed best performance with 100% Orange II decoloration compared to other mass compositions while bare TiO_2 showed only 21% Orange II decoloration. Among 9:1, 5:5 and 1:9 Cu:Ni mass compositions 1:9 Cu:Ni mass composition calcined at 200 °C gave 99.2% while 10:0 and 0:10 Cu: Ni mass compositions gave only 92.7% and 45.3% Orange II decoloration respectively. Comparison of Orange II decoloration vs %TOC removal with different Cu:Ni mass compositions and bare TiO_2 is shown in Figure 9.

It is well accepted that 100% decoloration of organic dyes such as Orange II does not mean that 100% mineralization of the dye. This is because during decoloration, many colorless long-lived intermediates, which might not be environmentally acceptable, are formed. Therefore, from the point of view of discharge standards, mineralization of Orange II could be equally important[23]. Detailed TOC analysis was conducted by further screening of the best performing photocatalysts for photodegradation studies to check the photocatalyst with highest performance with lower TOC values. In case of different Cu:Ni mass compositions 9Cu:1Ni-200 photocatalysts showed best performance with 100% Orange II decoloration and lowest TOC values 3.18 ppm (89.9 %) for 1 h reaction study compared to 5Cu:5Ni-200, 1Cu:9Ni-200, 10Cu:0Ni-200 and 0Cu:10Ni-200 photocatalysts with TOC values 22.9ppm, 12.9 ppm, 20.5 ppm and 25.8 ppm, respectively. After 1.5 h of irradiation duration, 9Cu:1Ni-200 photocatalyst was reported with the 100% TOC removal.

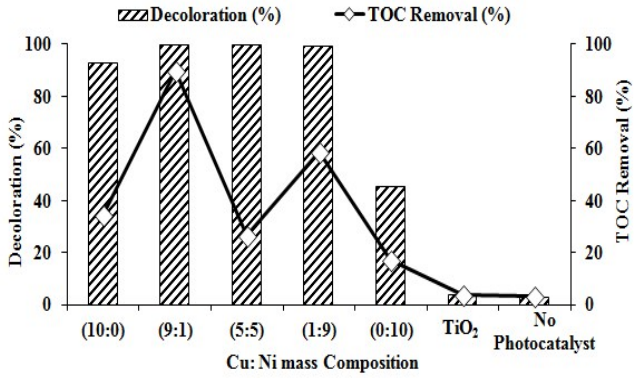

Fig.9 Effect of Cu:Ni mass compositionon % Orange II decoloration and %TOC removal (Reaction duration=1h)

Comparing the bandgap energies with the % Orange II decoloration during the photocatalytic reaction, results showed that there was not much significant difference for the calculated bandgap energies for all the photocatalysts. 10wt%-WI-9Cu:1Ni-300 was reported with the lowest bandgap energy (2.74eV) and 100% Orange II decoloration. The same photocatalyst was observed with 22.8 ppm TOC value that was higher compared to the best performing 10wt%- WI-9Cu:1Ni-200. This shows that the low bandgap energy alone was not the only factor affecting the photocatalytic activity.

Effect of calcination temperature. All the Cu-Ni/TiO_2 photocatalysts displayed better dye decoloration activity regardless of the calcination temperatures. The photocatalysts calcined at 180 °C, with 9:1 and 5:5 Cu:Ni mass compositions were observed with 100% Orange II decoloration and 1:9 Cu:Ni mass compositions calcined at 200 °C gave 99.2%. Although the photocatalyst performance was 100 % but the difference in performance was identified as the TOC removal efficiency. Comparison of % TOC removal for photocatalyst with different Cu:Ni mass compositions is shown in Figure 10. The best values obtained for photocatalyst calcined at 200° C with 100 % Orange II decoloration and 89.9 % TOC removal (3.18 ppm TOC value). The TOC % removal for different calcination temperature was 56.3 % and 27.2 % for photocatalysts calcined at 180 and 300 ° C, respectively. The results also indicate that the photocatalytic activity of synthesized titania decreased with the increased calcination temperature. Yu et al. [61] also reported a significant decrease in the photocatalytic activity of titanianopowder calcined at higher temperature may be attributed to the growth of particle and result in the reduction of contact area of particles for photocatalytic reaction. The improvement of photocatalytic activity compared with commercial materials can be associated to the combined increase of crystallinity with the preservation of a relatively large surface area based on the existence of mesopores[62].

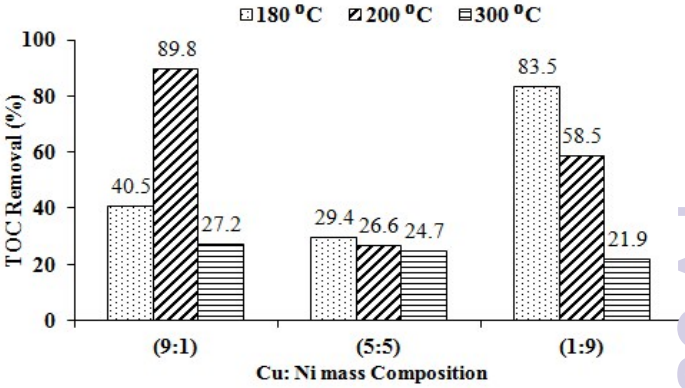

Fig.10 Effect of Cu-Ni mass composition on TOC for WI photocatalysts

Effect of initial pH. The interpretation of pH effects on the efficiency of dye photodegradation process is a very complex parameter task because of its multiple roles. 10 wt% Cu-Ni/TiO_2 photocatalysts with 9:1 Cu:Ni mass composition calcined at 200°C displayed the lowest dye degradation at pH 3 (22.3%) and the highest dye degradation at pH 6.8 (Figure 11). The effect of pH is generally dependent on the type of the pollutant and surface properties of the photocatalysts [27]. The effect of pH on the

photocatalytic degradation of Orange II can be explained by the surface charge of Cu-Ni/TiO_2 photocatalysts (positive) and its relation to the acid dye Orange II. In this study at pH 6.8, while the pH is neutral, a strong adsorption of the acid dye onto the photocatalysts particle as a result of electrostatic attraction of positively charged TiO_2 with the ionized dyes is observed. This can also be seen with the naked eye, while the photocatalyst turns orange-brown from light aquamarine color. On the other hand, above pH 6.8, a decrease in the reaction rate has been observed with a minimum at pH 12, reflecting the difficulty of anionic dye in approaching the negatively charged TiO_2 surface when increasing solution pH.At pH higher than PZC the photocatalyst surface was negatively charged, thus preventing the negatively charged dye as well as the hydroxide anion from adsorbing onto the surface, this would explain the reduced degree of degradation recorded at alkaline conditions. On the other hand, adsorption of negatively charged dye was favored at pH lower than the PZC due to the positively charged photocatalyst surface. In this study the higher percentage of dye decoloration was achieved at pH 6.8 and PZC value for Cu-Ni/TiO_2 is above pH 7.40 for higher metal oxides loading. Findings of others [27, 28] showed that degradation of anionic dyes is more in acidic medium, compared to pH equal or higher than PZC value of TiO_2. Furthermore using ZnO photocatalysts, degradation of Orange II are much faster in neutral medium [63]. So it can be said that pH equals to PZC of TiO_2 would favor the best results for Orange II decoloration with lower TOC values. After the photodegradation (60 min duration), the remaining TOC was different for different photocatalysts compared to their initial TOC values. In case of different initial pH for the reaction sample using 9Cu:1Ni-200, 100% decoloration with 89.8% TOC removal was observed at pH 6.8, the best performance as compared to other pH values.

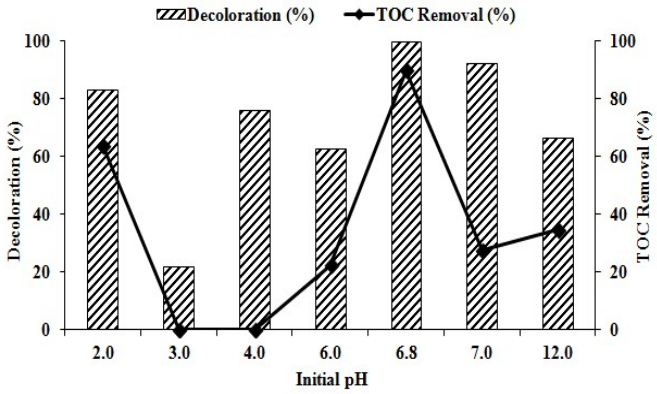

Fig.11 Effect of initial pHon Orange II decoloration

Effect of metal loading. By fixing the Cu-Ni mass composition (9Cu:1Ni-200), photocatalysts with different metal loading (5, 10 and 15 wt%) were screened for Orange II decoloration. For different metal loading 10wt% 9:1 Cu-Ni/TiO_2 photocatalysts showed best performance with 100% Orange II decoloration compared to 5wt% photocatalysts with 52.8% and 15wt% photocatalysts with 55.2% Orange II decoloration respectively (S8). As the metal loading increased, blockage of the active sites of TiO_2 may occur as the effect of excessive coverage which results in limitation of light penetration reaching the surface [9, 64]. Thus the number of photogenerated e^- and h^+ reduced and subsequently lowered the photocatalytic activity[65]. Furthermore, as the metal loading increases, agglomeration of metal particles is believed to occur that decrease the photocatalytic activity of photocatalyst[31, 55]. The optimum photocatalysts loading was obtained for photocatalysts with 10wt% that showed 89.8% TOC removal compared to 29.8ppm (4.7% TOC removal) and 35.3ppm (0% TOC removal) for 5 wt% and 15 wt% respectively.

Effect of photocatalysts loading. TiO_2 loading in slurry photocatalytic processes is an important factor that can influence dye degradation[38]. The effect of catalyst loading was studied for Orange II decoloration in the range 100–1000 mg·L^{-1} and the comparison of Orange II decoloration and %TOC removal is shown in S9. It was observed that photocatalysts loading is directly proportional to the Orange II decoloration[28, 66, 67]. With increasing concentration of photocatalysts, Orange II decoloration was also increased while TOC was decreased with increasing concentration of photocatalyst.

Effect of irradiation time. Orange II decoloration (%) as a function of time (120 min dark reaction followed by 60 min light reaction) for WI photocatalysts with 9:1 Cu:Ni mass composition calcined at different temperature is displayed in Figure 12. During dark reaction, decoloration was the fastest for photocatalyst calcined at 180ºC with 95.3% after the dark reaction without exposure to irradiation indicating high dye adsorption rate. For photocatalyst calcined at 200°C, Orange IIdecoloration was observed even in the dark, and the decoloration progressed to 89.4% after 120 min in the dark. The degradation progressed further to 100% after 60 min irradiation. However, for photocatalyst calcined at 300 ºC and bare TiO_2, degradation rate during dark reaction was very slow (61.8% and 37.4%) compared to other two photocatalysts which further increased to 100% and 21% after irradiation of 60 min, respectively. It is evident that the percentage of decoloration and photodegradation increases with irradiation time for photocatalysts calcined at different temperatures. Photocatalysts calcined at 300ºC showed less adsorption during dark reaction but the rate of reaction during irradiation was comparable to that for photocatalyst calcined at 200°C. The reaction rate during light reaction decreases with irradiation time as it follows the pseudo first-order kinetics and additionally a competition for degradation may occur between the reactant and the intermediate products. The slow kinetics of dye degradation after certain time limit is mainly attributed to: (a) the difficulty in converting the N-atoms in Orange II into oxidized nitrogen compounds [68], (b) the slow reaction of short chain aliphatics with •OH radicals [69] and (c) the short life-time of photocatalyst because of active sites deactivation by strong by-products deposition (carbon etc.) [70].

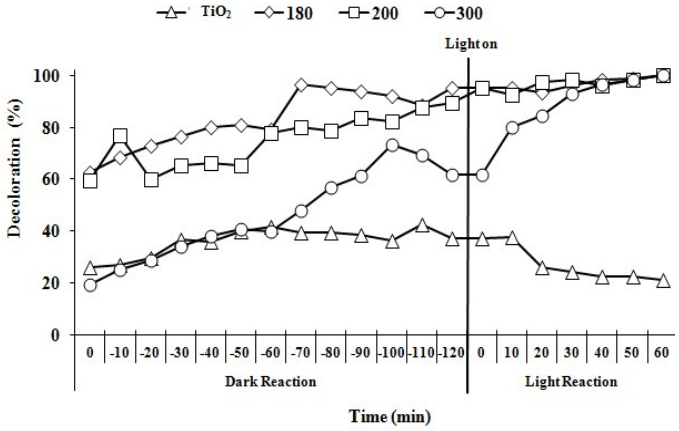

Fig.12 Orange II decoloration in the dark and under visible light irradiation using bare TiO_2 and WI photocatalysts with 9Cu:1Ni mass compostion calcined at different temperatures.

Table 3 Effects of different physical parameters on Orange II decoloration and TOC using selective photocatalysts and bare TiO_2

Photocatalysts	$[Org\ II]_f$ (ppm)	Decoloration (%)	TOC_f (ppm)	TOC Removal(%)
Bare TiO_2	39.5	21	55.7	4.0
NoPhotocatalyst	48.49	3.0	36.7	18.4
5wt%-9Cu:1Ni-200	23.6	52.8	29.8	4.7
15wt%-9Cu:1Ni-200	22.4	55.2	35.3	0.0
10wt%-10Cu:0Ni-200	3.6	92.7	20.5	34.5
10wt%-9Cu:1Ni-200	0	100	3.19	89.9
10wt%-5Cu:5Ni-200	0	100	22.9	26.6
10wt%-1Cu:9Ni-200	0.41	99.2	12.9	58.5
10wt%-0Cu:10Ni-200	27.4	45.3	25.9	17.3
10wt%-9Cu:1Ni-180	0	100	13.6	40.5
10wt%-5Cu:5Ni-180	0	100	16.08	29.4
10wt%-3Cu:7Ni-180	0	100	8.61	40.9
10wt%-1Cu:9Ni-180	0	100	4.19	83.5
10wt%-9Cu:1Ni-300	0	100	22.8	27.2

$[Org\ II]_f$= Final Orange II conc. in ppm after 1h; TOC_f = Final TOC value in ppm after 1h, pH=6.8]

UV–visible spectral changes. In order to understand and clarify the changes in molecular and structural characteristics of Orange II as a result of photodegradation using Cu-Ni/TiO_2 photocatalysts under visible light irradiation, representative UV–visible spectral changes in the dye solution as a function of irradiation time were observed and the corresponding spectra are shown in Figure 13 for 9Cu:1Ni-200 photocatalysts. It can be observed from UV–vis spectra at different time interval, the absorption spectrum of Orange II in water was characterized by one main band in the visible region, with its maximum absorption at 485 nm and by the other band in the ultraviolet region located at 310 nm, respectively. The peaks at 310 nm were associated with "benzene-like" structures in the molecule, and that at 485 nm originated from an extended chromophore, comprising both aromatic rings, connected through the azo bond. The absorbance peak at 485.0 nm was used as the representative peak for Orange II concentration[71-73]. After 30 min of irradiation time and onwards, the visible band the disappearance of the visible band was observed that might be due to the fragmentation of the azo links by oxidation [74]. In addition to this rapid decoloration effect, the decay of the absorbance at 310 nm was considered as evidence of aromatic fragment degradation in the dye molecule and its intermediates [72].

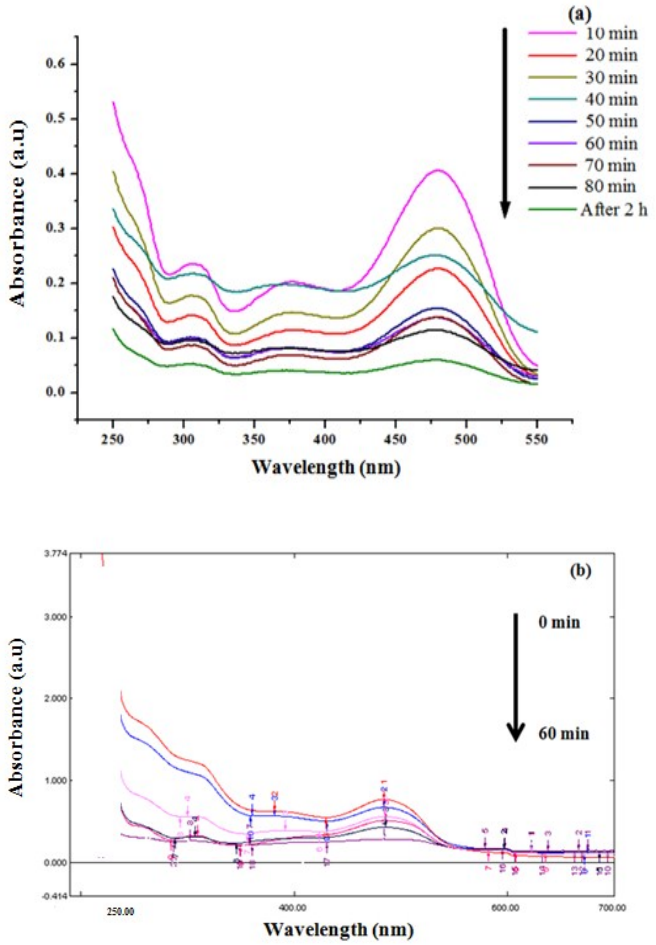

Fig.13 UV–vis spectra changes with reaction time (0 min- 60 min) for Orange II decoloration during (a) dark reaction and (b) light reaction

Analysis of intermediates and by-products

Reaction intermediate and final products at specific time interval of photocatalytic degradation reactions were identified by HPLC. Degradation products formed during the photodegradation process using visible light source were analyzed using HPLC. There are several separation peaks appearing during the degradation experiment, which can be ascribed to the intermediates of the Orange II dye degradation. Peaks were obtained for the intermediates compounds and final products such as Oxalic acid, formaldehyde, benzyl alcohol, benzaldehyde, salfanilic acid and formic acid [27, 28] and Salfanilic acid. From the Chromatogram of reaction samples before and after the photo-reaction (S10), it is clear that 1h of irradiation time was enough to remove Orange II

completely from the samples. The retention time of identified photodegradation compounds (using bimetallic photocatalysts and bare TiO_2 photocatalysts) detected after 1 h of irradiation time are presented in Table 4. The identified intermediates and by products are at RT 1.2 (oxalic acid), RT 1.4 (formic acid), RT 1.7 (formaldehyde), RT 3.8 (benzyl alcohol) and RT 7.8 (benzaldehyde).

Table 4Identified intermediates and by products obtained by Orange II decoloration

	Products	RT	Products identified in different reaction samples	
			WI	TiO_2
A	Oxalic Acid (OA)	1.2	✓	✓
B	Formic Acid (FA)	1.4	✓	✓
C	Formaldehyde (FD)	1.7	✓	X
D	N	1.8	X	✓
E	N	2.2	✓	✓
F	Benzyl Alcohol (BA)	3.8	✓	✓
G	N	2.4	X	✓
H	N	4.3	✓	✓
I	N	4.8	X	X
J	Benzaldehyde (BD)	7.5	✓	X

✓= Identified; RT= Retention time (min), N = Not identified; X= Not detected

Intermediates and products appeared during reaction at different time interval and pH value 6.8 may change in different trends, and therefore their contents as a function of time were measured and the plot of changing concentrations of the identified organic intermediates is shown in Figure 14.

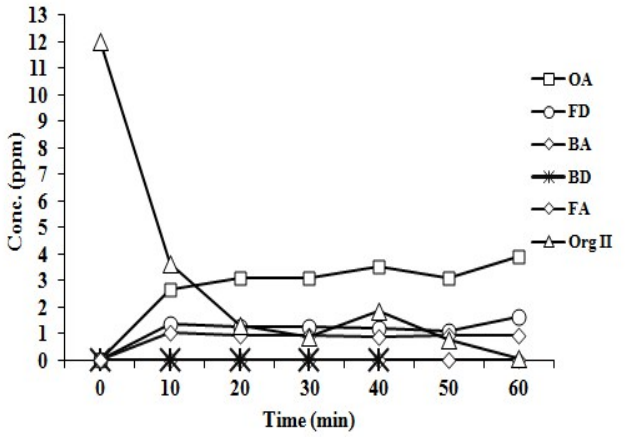

Fig.14 Intensity Changes in concentration of the organic compounds as a function of time at different retention time (irradiation duration= 1h)

Proposed Mechanism of Orange II photodegradation

Orange II is the most studied compound among the azo dyes as far as its photocatalytic degradation under several experimental conditions. The degradation pathways and the formation of by-products is also fully described in literature[27, 75-77]. In bimetallic photocatalysts, the addition of small amount of Ni, enhanced the activity of photocatalyst. Photocatalysts with higher Cu contents (e.g 9Cu:1Ni mass composition) showed higher activity compared to those of bimetallic photocatalyst with lower Cu content and monometallic photocatalysts. Cu^{2+}also acts as electron trap, adding small amount of Ni can enhance the hole trapping process thus retarding recombination reaction. However, as the amount of Ni increased, it becomes hole accumulation site. Such hole accumulation further attracted the negatively charged species, either from one embodied in Cu^{2+} (as electron trap) or the mobile electron from the conduction band of TiO_2. Therefore, Ni^{2+} itself becomes the recombination reaction center thus decreasing the activity of photocatalyst. A decrease in Cu content led to lower Orange II decoloration. Meanwhile, for monometallic 10Cu:0Ni-200 and 0Cu:10Ni-200, the activities were found to be lower than those of some bimetallic Cu-Ni/TiO_2 photocatalysts [9, 78].

Degradation of Orange II was found to increase with increasing the photocatalyst concentration and at neutral pH of the solution. As discussed previously the photocatalytic degradation by products can be classified into three groups: (i) naphthalene like compounds such as 2-napthole which is a primary degradation intermediates accompanying Orange II cleavage in the vicinity of the azo bond [75, 76]. Its formation has also been corroborated in several previous studies concerning Orange II photocatalytic degradation [28], (ii) aromatic intermediates such as benzyl alcohol, benzaldehyde, 2-methyl phenol, toluene and benzophenone and (iii) ring cleavage compounds such as 2-ethyl-1-hexanol. Photocatalytically treated Orange II solution mainly consisted of aromatic intermediates as confirmed by HPLC analysis. The identified intermediates and by products are benzaldehyde, benzyl alcohol, formaldehyde, oxalic acid and formic acid. In photocatalytic oxidation process, active electron contribute to the decoloration and mineralization of the dye due to the producing of oxidative species such as $O_2^{\bullet-}$ and $^{\bullet}OOH$, but also contribute to the decoloration of Orange II as reductive species. After 60 min of irradiation, the reaction mixture consists of aliphatic compounds presumably due to the oxidation of Orange II and its ring intermediates. It is also assumed that the differences in the identified by-products of photocatalysis are due to the different photodegradation mechanisms involved.

On the other hand, the formation of these acids suggests the degradation process after the opening of aromatic and naphthalene rings. Once the azo bond is cleaved, the conjugated structure of Orange II dye is destructed, accompanied by the complete color removal rather than TOC removal. The most possible reduction mechanism is generally presented in the Figure 15. These results indicate that many intermediate compounds are converted into CO_2 via either formic acid. However since formic acid is photocatalytically more degradable than other aliphatic acids reported previously [77], the more intermediate compounds apparently degraded through formic acid. The complete degradation pathway of Cu-Ni/TiO_2 mediated photodegradation under visible light can be briefly summarized as:

View Article Online
DOI: 10.1039/C6RA10371E

$$\text{Dye} \rightarrow \text{intermediates} \rightarrow \text{aliphatic and aromatic acids} \rightarrow CO_2, NH_4^+, NO_3^-, NO_2^-, SO_4^{2-}$$

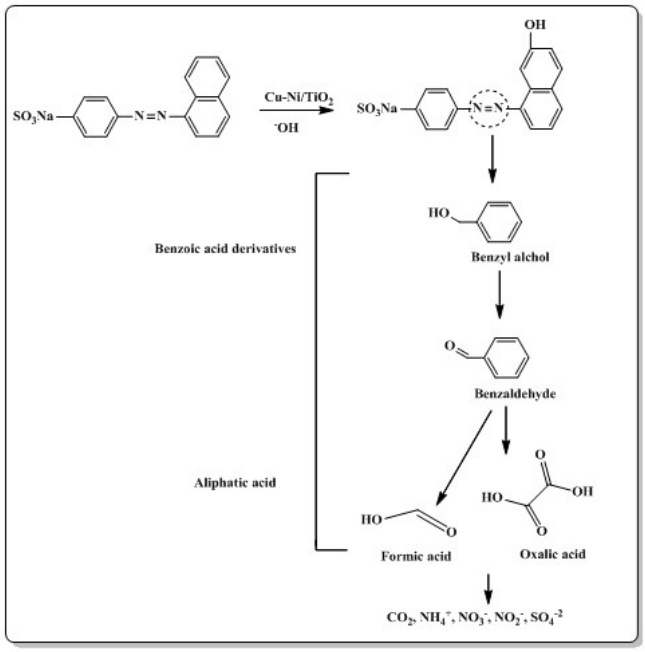

Fig.15 Proposed photodegradation mechanism of Orange II under visible light using Cu-Ni/TiO_2 photocatalyst

Photocatalyst recycling study

To investigate the recyclability/reusability of the photocatalyst after reaction study, photocatalytic degradation study was carried out for multiple times using recycled photocatalyst and the results for the Orange II decoloration and TOC removal (%) are presented in the Figure 16. It was found that the activity of photocatalyst decreased as the recycle number increased which was showed by the decreased % Orange II photodegradation. Results for Orange II decoloration was 100% with 89.8% TOC removal, when photocatalysts was used for the first time and reduction peaks at 289 and 357°C with 1879.4 and 1938.2μmol·g^{-1} hydrogen consumption. After the first reaction study, the Orange II % decoloration was decreased up to 83.98% and 58.4% TOC removal. The percent dye decoloration was still higher (75.6%Orange II decoloration and 46.3% TOC removal) compared to that obtained with bare TiO_2.

In S11, the reduction peak for recycled photocatalyst was found at lower temperature (185 and 263°C with 163.3 and 142.0 μmol·g^{-1}, low hydrogen consumption) compared to fresh photocatalyst. The enhanced reducibility of the photocatalyst might be ascribed to the interaction between CuO and NiO with TiO_2. The interaction between CuO and NiO with TiO_2 reduce as the photocatalyst used for sequence of reaction. In S12 FTIR spectra comparison of Orange II dye, fresh and used photocatalysts are shown, indicating that even after two washings still a small amount of dye was detectable. The decrease in the efficiency of the recycled catalyst may be attributed to the deposition of photoinsensitive hydroxides (Fouling) on the photocatalysts surface blocking its active sites [79].

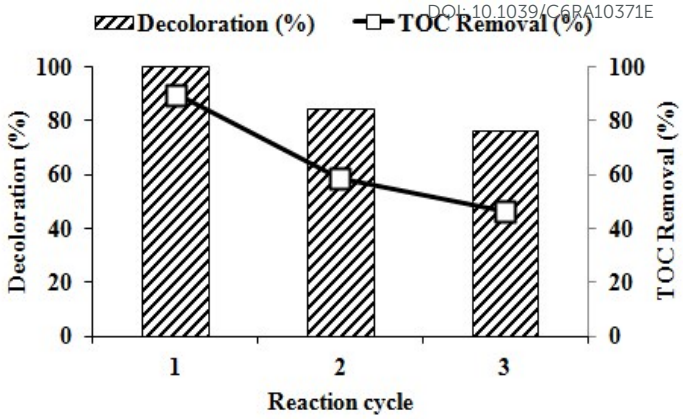

Fig.16 Photocatalyst recycling study: Orange II % decoloration (irradiation duration= 1h)

Conclusions

In this study, a series of monometallic and bimetallic Cu-Ni/TiO_2photocatalysts were successfully prepared wet impregnation (WI) methods for Orange II removal. Photocatalysts with different Cu-Ni mass compositions (10:0, 9:1, 7:3, 5:5, 3:7, 1:9 and 0:10) with different total metal loading (5, 10 and 15 wt%) were prepared. The physical and chemical properties of the modified Cu-Ni doped photocatalysts and bare TiO_2 were investigated and it was concluded that the addition of metal onto the surface of TiO_2 has successfully modified the physical and chemical properties of bare TiO_2 which led to better photocatalytic performance for Orange II photodegradation activity under visible light irradiation. For the photocatalysts samples containing Cu and Ni, the PZC shifts to more basic values (7.7) compared to that of the support (for TiO_2 was about 3.8). In XRD analysis, no phase transition was observed for anatase into rutile for the calcined photocatalysts and also no diffraction lines of Cu or Ni containing phases were observed indicating that the dopants were well dispersed onto TiO_2. FESEM and HRTEM analysis for all the samples showed spherical and agglomerated morphologies. DRUV-Vis analysis showed that incorporation of Cu and Ni onto TiO_2 has successfully shifted the optical absorption to the visible region with reduced bandgap energies.

The synthesized Cu-Ni/TiO_2 photocatalysts were screened for Orange II dye decoloration efficiency against different reaction parameters. The photocatalyst activity is directly related to photocatalysts loading while the optimum pH for Orange II decoloration was pH 6.8 with the best performance (100% Orange II decoloration). Higher calcination temperature (300°C) resulted $TiO_{2\ \text{photocatalysts}}$ with lower bandgap energy 2.74 eV for 9Cu:1Ni-300. Despite of some advantages, some detrimental effects such as decreased performance for Orange II mineralization were observed. For different Cu:Ni mass compositions and metal loading, 10wt%-9Cu:1Ni photocatalysts showed the best performance with 100% Orange II decoloration with 10 wt% optimum metal loading and 9Cu:1Ni mass composition. The improvement in catalytic performance can also be attributed to the synergistic effect of

reduced bandgap energy, high crystallinity, smaller particle size, increase in surface area and to the higher number of OH groups exposed on the surface of the Cu-Ni-metalized TiO_2. Therefore, enhanced photocatalytic activity of the Cu-Ni/TiO_2 photocatalysts was observed under the present experimental conditions. The main identified intermediates and by products of Orange II photodegradation under visible light irradiation during reaction as a function of time were oxalic acid, formic acid, formaldehyde, benzyl alcohol and benzaldehyde as measured by HPLC analysis. The as-prepared Cu-Ni/TiO_2 photocatalysts have a great potential for photocatalytic water purification, particularly the elimination of toxic aromatic compounds. Highly stable Cu-Ni/TiO_2 photocatalysts with excellent responsiveness to visible light (wavelength and the efficiency of maximum absorbance) might be beneficial for solar-driven applications in the treatment of hazardous aqueous pollutants and might play an important role as ''green'' and inexpensive photocatalysts for the improvement of water quality.

Acknowledgments

The authors would like to acknowledge Universiti Teknologi PETRONAS for the funding of this research work.

References

1. M. S. Secula, G. D. Suditu, I. Poulios, C. Cojocaru and I. Cretescu, *Chemical Engineering Journal*, 2008, **141**, 18-26.
2. P. A. Carneiro, M. E. Osugi, J. J. Sene, M. A. Anderson and M. V. B. Zanoni, *Electrochimica Acta*, 2004, **49**, 3807-3820.
3. R. J. Maguire, *Water Sci. Technol.*, 1992, **26**, 265-270.
4. S. Meric, D. Kaptan and T. Olmez, *Chemosphere*, 2004, **54**, 435–441.
5. C. M. Carliell, S. J. Barclay and C. A. Buckley, *Microbial decolourization of a reactive azo dye under anaerobic conditions*, Report 863, Water Research Commission South Africa, 1995.
6. M. Halmann, *Photodegradation of Water Pollutants*, CRC Press: Boca Raton, FL, 1996.
7. H. Lachheb, E. Puzenat, A. Houas, M. Ksibi, E. Elaloui, C. Guillard and J.-M. Herrmann, *Applied Catalysis B: Environmental*, 2002, **39**, 75-90.
8. M. R. Hoffmann, S. T. Martin, W. Choi and D. W. Bahnemann, *Chemical Reviews*, 1995, **95**, 69-96.
9. O. Carp, C. L. Huisman and A. Reller, *Progress in Solid State Chemistry*, 2004, **32**, 33-117.
10. A. Fujishima, T. N. Rao and D. A. Tryk, *Journal of Photochemistry and Photobiology C: Photochemistry Reviews*, 2000, **1**, 1-21.
11. M. Anpo and M. Takeuchi, *Journal of Catalysis*, 2003, **216**, 505-516.
12. D. Zhang, *Monatshefte für Chemie/Chemical Monthly*, 2012, **143**, 729-738.
13. D. Zhang and F. Zeng, *Applied Surface Science*, 2010, **257**, 867-871.
14. N. Riaz, M. A. Bustam, S. Ullah, A. E. Elkhalifah, G. Gonfa and A. M. Shariff, 2016.
15. Y. Liu and D. Liu, *International Journal of Hydrogen Energy*, 1999, **24**, 351-354.
16. T.-J. Huang and S.-Y. Jhao, *Applied Catalysis A: General*, 2006, **302**, 325-332.
17. I. Gandarias, J. Requies, P. L. Arias, U. Armbruster and A. Martin, *Journal of Catalysis*, 2012, **290**, 79-89.
18. M. J. Lázaro, Y. Echegoyen, I. Suelves, J. M. Palacios and R. Moliner, *Applied Catalysis A: General*, 2007, **329**, 22-29.
19. W. Gao, R. Jin, J. Chen, X. Guan, H. Zeng, F. Zhang and N. Guan, *Catalysis Today*, 2004, **90**, 331-336.
20. D. Zhang and F. Zeng, *Russian Journal of Physical Chemistry A, Focus on Chemistry*, 2011, **85**, 1077-1083.
21. D. Zhang, *Journal of Sol-Gel Science and Technology*, 2011, **58**, 312-318.
22. D. Zhang, *Transition Metal Chemistry*, 2010, **35**, 933-938.
23. R. S. K. Wong, J. Feng, X. Hu and P. L. Yue, *Journal of Environmental Science and Health, Part A: Toxic /Hazardous Substances and Environmental Engineering*, 2004, **39**, 2583 - 2595.
24. N. Riaz, F. K. Chong, B. K. Dutta, Z. B. Man, M. S. Khan and E. Nurlaela, *Chemical Engineering Journal*, 2012, **185–186**, 108-119.
25. N. Riaz, F. K. Chong, Z. B. Man, M. S. Khan and B. K. Dutta, *Industrial & Engineering Chemistry Research*, 2013, **52**, 4491-4503.
26. A. Di Paola, E. García-López, G. Marcì, C. Martín, L. Palmisano, V. Rives and A. Maria Venezia, *Applied Catalysis B: Environmental*, 2004, **48**, 223-233.
27. I. K. Konstantinou and T. A. Albanis, *Applied Catalysis B: Environmental*, 2004, **49**, 1-14.
28. T. Velegraki, I. Poulios, M. Charalabaki, N. Kalogerakis, P. Samaras and D. Mantzavinos, *Applied Catalysis B: Environmental*, 2006, **62**, 159-168.
29. R. Brás, A. Gomes, M. I. A. Ferra, H. M. Pinheiro and I. C. Gonçalves, *Journal of Biotechnology*, 2005, **115**, 57-66.
30. G. Li, J. Qu, X. Zhang, H. Liu and H. Liu, *Journal of Molecular Catalysis A: Chemical*, 2006, **259**, 238-244.
31. L. S. Yoong, F. K. Chong and B. K. Dutta, *Energy*, 2009, **34**, 1652-1661.
32. H. Tanaka and T. Sadamoto, *Thermochimica Acta*, 1982, **54**, 273-280.
33. J. Sun, Y. Jing, Y. Jia, M. Tillard and C. Belin, *Materials Letters*, 2005, **59**, 3933-3936.
34. D. Li, H. Haneda, S. Hishita and N. Ohashi, *Materials Science and Engineering: B*, 2005, **117**, 67-75.
35. X. Yan, J. He, D. G. Evans, Y. Zhu and X. Duan, *Journal of Porous Materials*, 2004, **11**, 131-139.
36. R. Linacero, J. Aguado-Serrano and M. Rojas-Cervantes, *Journal of Materials Science*, 2006, **41**, 2457-2464.
37. K. Porkodi and S. D. Arokiamary, *Materials Characterization*, 2007, **58**, 495-503.
38. J. Mohan, *Organic Spectroscopy Principles and Applications*, Harrow,U.K.: Alpha Science International Ltd., 2nd edn., 2007.
39. J. L. Li and T. Inui, *Applied Catalysis A: General*, 1996, **137**, 105-117.
40. J.-P. Jolivet, Marc Henry and J. Livage, *Metal Oxide Chemistry and Synthesis – From Solution to Solid State*, John Wiley & Sons Ltd.,Chichester, 2000., 2000.
41. A. Di Paola, S. Ikeda, G. Marcì, B. Ohtani and L. Palmisano, *International Journal of Photoenergy*, 2001, **3**, 171-176.
42. A. Di Paola, G. Marcì, L. Palmisano, M. Schiavello, K. Uosaki, S. Ikeda and B. Ohtani, *The Journal of Physical Chemistry B*, 2002, **106**, 637-645.
43. A. Bauer, K. Lee, C. Song, Y. Xie, J. Zhang and R. Hui, *Journal of Power Sources*, 2010, **195**, 3105-3110.

44. M. Xie, L. Jing, J. Zhou, J. Lin and H. Fu, *Journal of Hazardous Materials*, 2010, **176**, 139-145.
45. T. Sreethawong, Y. Suzuki and S. Yoshikawa, *International Journal of Hydrogen Energy*, 2005, **30**, 1053-1062.
46. H. Zhu, Y. Wu, X. Zhao, H. Wan, L. Yang, J. Hong, Q. Yu, L. Dong, Y. Chen, C. Jian, J. Wei and P. Xu, *Journal of Molecular Catalysis A: Chemical*, 2006, **243**, 24-30.
47. E. I. Ko, *Sol-gel Process, in Handbook of heterogeneous catalysis*, VCH Verlagsgesellschaft mbH: Weinheim., 1997.
48. T. Lopez, E. Sanchez, P. Bosch, Y. Meas and R. Gomez, *Materials Chemistry and Physics*, 1992, **32**, 141-152.
49. N. Riaz, M. A. Bustam, F. K. Chong, Z. B. Man, M. S. Khan and A. M. Shariff, *The Scientific World Journal*, 2014, **2014**.
50. E. Nurlaela, F. K. Chong, B. K. Dutta and N. Riaz, presented in part at the International Conference on Fundamental and Applied Sciences (ICFAS2010), Kuala Lumpur, Convention Center, Kuala Lumpur, 15 to 17 June 2010, 2010.
51. S. Xu, J. Ng, X. Zhang, H. Bai and D. D. Sun, *International Journal of Hydrogen Energy*, 2010, **35**, 5254-5261.
52. S. Rahimnejad, S. S. Rahman and M. R. Gholami, *Journal of Iranian Chemical Society*, 2008, **5**, 367-374.
53. K. S. W. Sing, D. H. Everett, R. A. W. Haul, L. Moscou, R. A. Pierotti, J. Rouquerol and T. Siemieniewska., *Pure & Appl. Chem.*, 1985, **57**, 603—619.
54. G. Marci, L. Palmisano, A. Sclafani, A. M. Venezia, R. Campostrini, G. Carturan, C. Martin, V. Rives and G. Solana, *Journal of the Chemical Society, Faraday Transactions*, 1996, **92**, 819-829.
55. E. Nurlaela, Maters Thesis, Universiti Teknologi PETRONAS, 2011.
56. J. Wade, MSc thesis, University of South Florida, 2005.
57. M. D. Fuerte, Hern´andez-Alonso, A. J. Maira, A. Mart´ınez-Arias, M. Fern´andez-Garc´ıa, J. C. Conesa, J. Soria and G. Munuera, *Journal of Catalysis*, 2002, **212**, 1-9.
58. S. Sakthivel, M. C. Hidalgo, D. W. Bahnemann, S. U. Geissen, V. Murugesan and A. Vogelpohl, *Applied Catalysis B: Environmental*, 2006, **63**, 31-40.
59. M. D. Romero, J. A. Calles, A. Rodríguez and J. C. Cabanelas, *Industrial & Engineering Chemistry Research*, 1998, **37**, 3846-3852.
60. P. Li, J. Liu, N. Nag and P. A. Crozier, *Journal of Catalysis*, 2009, **262**, 73-82.
61. J. C. Yu, J. Lin, D. Lo and S. K. Lam, *Langmuir*, 2000, **16**, 7304-7308.
62. S. Sakulkhaemaruethai, S. Pavasupree, Y. Suzuki and S. Yoshikawa, *Materials Letters*, 2005, **59**, 2965-2968.
63. N. Daneshvar, M. H. Rasoulifard, A. R. Khataee and F. Hosseinzadeh, *Journal of Hazardous Materials*, 2007, **143**, 95-101.
64. H. M. Coleman, K.Chiang and R.Amal, *Chemical Engineering Journal*, 2005, **113**, 65–72.
65. M. A. Behnajady, N. Modirshahla, M. Shokri and B. Rad, *Global NEST Journal*, 2008, **10**, 1-7.
66. M. N. Chong, B. Jin, C. W. K. Chow and C. Saint, *Water Research*, 2010, **44**, 2997-3027.
67. F. Chen, Y. Xie, J. Zhao and G. Lu, *Chemosphere*, 2001, **44**, 1159-1168.
68. J. Bandara, V. Nadtochenko, J. Kiwi and C. Pulgarin, *Water Science and Technology*, 1997, **35**, 87–93
69. C. Walling, *Accounts of Chemical Research*, 1975, **8**, 125-131.
70. Y. Li, S. Sun, M. Ma, Y. Ouyang and W. Yan, *Chemical Engineering Journal*, 2008, **142**, 147–155.
71. K. Bourikas, C. Kordulis and A. Lycourghiotis, *Environmental Science & Technology*, 2005, **39**, 4100-4108.
72. F. Kiriakidou, D. I. Kondarides and X. E. Verykios, *Catalysis Today*, 1999, **54**, 119-130.
73. Y. Zhiyong, M. Bensimon, V. Sarria, I. Stolitchnov, W. Jardim, D. Laub, E. Mielczarski, J. Mielczarski, L. Kiwi-Minsker and J. Kiwi, *Applied Catalysis B: Environmental*, 2007, **76**, 185-195.
74. H. Zhang, Y. Zhang and D.B. Zhang, *Color. Technol.*, 2007, **123**, 101–105.
75. M. Stylidi, D. I. Kondarides and X. E. Verykios, *Applied Catalysis B: Environmental*, 2003, **40**, 271-286.
76. M. Stylidi, D. I. Kondarides and X. E. Verykios, *Applied Catalysis B: Environmental*, 2004, **47**, 189-201.
77. K. Tanaka, K. Padermpole and T. Hisanaga, *Water Research*, 2000, **34**, 327-333.
78. D. Y. C. Leung, C. W. X. Fu, M. Ni, M.K.H. Leung, X. Wang and X. Fu, *ChemSusChem*, 2010, 1 – 15.
79. S. A. Abo-Farha, *Journal of American Science*, 2010, **6**, 130-142.

View Article Online
DOI: 10.1039/C6RA10371E

Graphical Abstract